Static screening lengths in the gluon plasma

Thomas A. DeGrand
Physics Department, University of Colorado, Boulder, Colorado 80309

Carleton E. DeTar
Physics Department, University of Utah, Salt Lake City, Utah 84112

(Received 5 May 1986)

We report results of an extensive numerical simulation in lattice gauge theory to study various static screening lengths in a finite-temperature pure gluon plasma. Measurements are made for fixed triplet charges (Wilson lines) and a variety of local operators near and above the phase transition for lattices with $N_t=4$, 6, and 8. We find evidence for a sharp rise in the Wilson-line screening length near the phase transition, but not in screening lengths associated with other operators. We also find evidence for a possible scaling of the inverse screening lengths with temperature above the phase transition. Our results support the proposition that the gluon plasma has a complex structure, and suggest that its long-range nonhydrodynamic excitations just above the phase transition are associated with a color-singlet plasmonlike mode.

I. INTRODUCTION

The quark-gluon plasma has long attracted interest as a novel form of matter with unusual properties.[1] Although there is no convincing evidence that the plasma has been produced in the laboratory, efforts are under way to develop the high-energy heavy-ion beams thought to be necessary to bring about the conditions for its creation. The plasma is of cosmological interest as well, very likely having occurred in the early moments of the Universe.

Despite the considerable theoretical effort that has been devoted to the phenomenology of the plasma, very little is actually known about its properties that follow rigorously from quantum chromodynamics (QCD). It is expected from asymptotic freedom that at extremely high temperatures the plasma may be described to a good approximation as a gas of weakly interacting quarks and gluons.[2] Numerical simulations suggest that there may be a phase transition between a low-temperature hadronic gas and a high-temperature plasma phase.[3] However, at temperatures achievable in heavy-ion collisions, temperatures not much greater than that of the phase transitions, asymptotic freedom does not apply, and the weakly interacting gas model is surely inadequate.

Indeed, we really do not even know what the plasma is made of at the experimentally accessible temperatures, i.e., we do not know its elementary modes of excitation. Obviously, it is ultimately made of quarks and gluons, just as are the hadrons. But the excitations of the plasma are very likely not simply quasiquarks and quasigluons in analogy to a weakly interacting quantum-electrodynamic (QED) plasma. Without knowledge of the plasma structure, it is difficult to say with confidence what phenomena signal the formation of a plasma in a heavy-ion collision.

We undertake here to study, through a numerical Monte Carlo simulation, a set of quantities related to these elementary excitations, namely, the static screening lengths of the gluon plasma. These are found by measuring the decay of static correlation functions at large spacelike separation in the Gibbs ensemble at a fixed temperature. The simplest such correlation involves the interaction of a pair of fixed color-triplet and antitriplet charges, i.e., Wilson lines. The associated screening length is similar to the Debye length in QED and the corresponding dynamical excitation would be the plasmon in QED. Thus studying the static screening length gives indirect information about the elementary excitations. Because the plasma is strongly interacting and perhaps even confining in a sense,[4] the analogy with Debye screening in QED is very loose.

The organization of this report is as follows. In Sec. II below we discuss in more detail the relationship between the quantities measured and the dynamical excitations. We also discuss how the screening lengths may be expected to depend on temperature. In Sec. III we describe the numerical simulation and method of analysis. In Sec. IV we discuss our results. Conclusions and suggestions for future work are given in Sec. V.

II. "DYNAMICAL CONFINEMENT" IN THE QCD PLASMA

The modes of excitation of a statistical ensemble are found by studying its response to a disturbance and may be characterized by a correlation function

$$S_{AB}(k,\omega)=\int_{-\infty}^{\infty} d^3x \int_{-\infty}^{\infty} dt\, e^{i(\omega t-\mathbf{k}\cdot\mathbf{x})}[\langle A(\mathbf{x},t)B(0,0)\rangle-\langle A(0,0)\rangle\langle B(0,0)\rangle] \tag{2.1}$$

for a pair of local operators A and B (Ref. 5). Here $\langle\ \rangle$ denotes an ensemble average. The spectral function is defined as

$$\rho_{AB}(k,\omega)=(1\mp e^{-\beta\omega})S_{AB}(k,\omega)\ , \tag{2.2}$$

where the plus sign is for bosons and the minus sign for fermions. The spectral function may have peaks at low k and ω corresponding to stable or nearly stable modes of excitation of the system. The peaks in $\rho(k,\omega)$ correspond to poles in the retarded momentum-space propagator:

$$i\Gamma_R(\mathbf{k},\omega)=\int d^3x\int_0^\infty dt\, e^{i(\omega t-\mathbf{k}\cdot\mathbf{x})}\langle[A(\mathbf{x},t),B(0,0)]_\mp\rangle\ . \tag{2.3}$$

Each such pole occurs on a trajectory in $\mathbf{k},\omega,T$ defined by a dispersion relation

$$f(\mathbf{k},\omega,T)=0\ . \tag{2.4}$$

The standard definition of confinement refers to the response of the pure gluon plasma to the introduction of static triplet charges. The pure gluon plasma is *statically* deconfined at high temperature: the force between static triplet charges is Debye screened. However, one of us[4] has argued that the high-temperature plasma is *dynamically* confined, in the sense that any attempt to produce a long-range color-nonsinglet disturbance yields a disturbance that can also be generated by a color-singlet source. In the example above, if A and B are nonsinglet operators, suitable gauge fixing is done, and a narrow peak in $\rho_{AB}(k,\omega)$ is found, the peak will also be seen with some other choice of color-singlet operators A' and B'. On the other hand, if singlet and nonsinglet operators have distinguishable spectra, then the plasma is dynamically deconfined.

Whether or not the high-temperature plasma is dynamically confined depends partly on whether or not large spacelike Wilson loops obey an area law. In a (continuum) photon gas they do not; in a gluon gas they do (at least in lattice gauge theory).[6] The connection between dynamic confinement and spacelike loops is most easily seen at large spacelike separation. To make the correlation function gauge invariant, each quark may be attached to a string which runs off to infinity. (See Fig. 1.) To prevent this correlation function from vanishing due to the resulting large-area Wilson loop it is necessary for an antiquark to appear in the ensemble with a world line close to the world line of the quark. But in that case the disturbance propagating between the points is a color-singlet quark-antiquark bound state—a meson. Similar arguments can be made for color-octet sources. The spacelike correlation length is the screening length.

This argument, made for a Euclidean gauge theory, suggests that the imaginary time propagator

$$S_{AB}(k,i\omega_n)=\int_0^\beta d\tau\int d^3x\, e^{i\omega_n\tau}e^{-i\mathbf{k}\cdot\mathbf{x}}[\langle A(\mathbf{x},-i\tau)B(0,0)\rangle-\langle A(0,0)\rangle\langle B(0,0)\rangle] \tag{2.5}$$

should have only color-singlet poles in k when $\omega_n=0$. The poles occur at $k=\pm i\mu(T)$ where $\mu(T)$ is the inverse static screening length. It is plausible that each such pole lies on one of the trajectories (2.4) so that there is a one-to-one correspondence between real-time excitations and static screening lengths. The poles in k for discrete $i\omega_n$ correspond to the eigenstates of the spacewise transfer matrix, or equivalently, lie in the spectrum of SU(3) defined on a space-time manifold with one periodic compact space dimension of period $1/T$.

To find the lowest-lying pole $\mu(T)$ for $\omega_n=0$ we will measure (using Monte Carlo calculations) the time-averaged operator

$$\begin{aligned}S_{AB}(\mathbf{x})&=\langle A(\mathbf{x})B(0)\rangle-\langle A(0)\rangle\langle B(0)\rangle\\&\equiv\langle A(\mathbf{x})B(0)\rangle_{\rm conn}\ ,\end{aligned} \tag{2.6}$$

where

$$A(\mathbf{x})=\frac{1}{\beta}\int_0^\beta d\tau\, A(\mathbf{x},-i\tau)\ . \tag{2.7}$$

Since $S_{AB}(\mathbf{x})$ is the Fourier transform of $S_{AB}(k,i\omega_n=0)$ it will fall off at long distances like

$$S_{AB}(\mathbf{x})\sim\exp[-\mu(T)|\mathbf{x}|]/|\mathbf{x}|\ , \tag{2.8}$$

where $1/\mu(T)$ is the longest screening length associated with states excited by A and B.

Suggestive arguments for the origin of the area law for spacelike loops and hence for dynamic confinement can be made in weak and strong coupling. They are based on the idea of dimensional reduction. In a Euclidean functional integral for a gauge theory at high temperature the imaginary time axis has a periodic domain $0<\tau<1/T$. Nadkarni, Applequist, and Pisarski[7] have shown that at high temperature only bosonic modes that are static in τ contribute to low-momentum low-frequency Green's functions. Therefore the theory compactifies to three Euclidean dimensions. The three-dimensional theory is an SU(3) adjoint Higgs model, whose gauge fields $\mathbf{A}$ are the spacelike components of the vector potential in the original four-

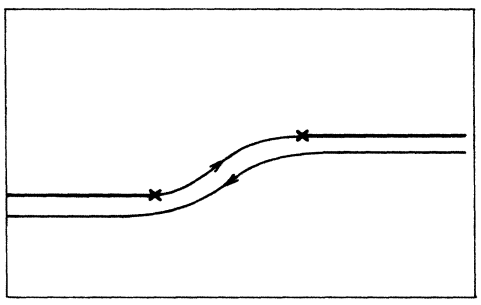

FIG. 1. Quark propagation diagram showing string location (heavy line) and possible world lines for a quark and antiquark (thin line).

dimensional theory. The Higgs field ϕ is the time component of the original vector potential. At high temperature the Higgs field develops a perturbative mass gT through Debye screening; g is the gauge coupling constant. The (dimensionful) coupling constant of the three-dimensional theory is g^2T. The same phenomenon has been shown to occur in the strongly coupled lattice theory by DeTar.[4] The three-dimensional gauge theory arising from dimensional reduction is believed to be confining for all values of its coupling constant $g_3{}^2=g^2T$ (Ref. 8). Its spectrum includes a set of bound states of the A field of mass $O(g^2T)$. This confining force is the origin of the area law for spacelike Wilson loops. It also binds the ϕ fields together into a color-singlet meson of mass $O(gT)$: most of the meson's mass is given by the plasmon mass. One also expects bound states of ϕ and A fields with mass $O(g^2T+gT)$.

Polonyi and Wyld[9] have argued that there is a dynamical breakdown of the SU(3) gauge symmetry for $T>T_c$ in a pattern similar to the three-dimensional Euclidean Georgi-Glashow model.[10] To have such an effect would require higher-order perturbative corrections to reverse the low-order positive squared mass of the color plasmon. They have presented some numerical evidence supporting their suggestion. Should there indeed be such a breakdown of the symmetry, the resulting compact Abelian theory would nonetheless very likely be confining as argued by Polyakov.[11]

With the above qualitative picture in mind, let us consider the possible spectrum of a variety of operators. The pure gluon plasma undergoes a first-order static deconfinement phase transition at a temperature $T=T_c$. The order parameter for static deconfinement is the Wilson line or Polyakov loop

$$\langle L(\mathbf{x})\rangle=\left\langle \mathrm{Tr}\exp\left[\int_0^\beta ig\phi^a(\mathbf{x})\lambda^a d\tau\right]\right\rangle \tag{2.9}$$

which is zero for $T<T_c$ and nonzero for $T>T_c$. With the functional integral turned on its side, i.e., switching the roles of one space axis and the imaginary time axis, the Wilson line may be interpreted as an operator that creates a loop of color-triplet flux, a "fluxon," which is closed due to the periodicity of the lattice. This object is created from the T-dependent vacuum of the spacewise transfer matrix. For $T<T_c$ the expectation value of $L(x)$ vanishes, so these states are orthogonal to the vacuum. Moreover, these states are orthogonal to any states created from the vacuum by a local operator, such as a small Wilson loop. For $T>T_c$, $\langle L\rangle\neq 0$ and the vacuum can contain an arbitrary number of these states. These states mix with states created by local operators. Near zero temperature the fluxon mass is determined by the string tension so that[12]

$$\mu_{\mathrm{WL}}(T)\approx\kappa/T-\frac{\pi}{3}T\ . \tag{2.10}$$

Thus the Wilson line or Debye screening mass decreases from infinity as T increases from zero. It is not known whether the fluxon necessarily corresponds to a dynamically propagating plasma mode for $T<T_c$. However, for $T>T_c$ it is expected to propagate, since it mixes with the glueball analogs produced by local operators.

Let us call this spacewise fluxon a *color-singlet plasmon*, in loose analogy with the plasmon in QED.

For high temperature and weak coupling we may expand $L(\mathbf{x})$ in $\beta=1/T$. In a static gauge ($d\phi^a/d\tau=0$)

$$L(\mathbf{x})\sim 3-g^2\beta^2|\phi^a(x)|^2\ . \tag{2.11}$$

Thus the Wilson line creates a color-singlet state of two ϕ fields. Because ϕ is massive, the correlation function of L with L decays like

$$\langle L(x)L(0)\rangle_{\mathrm{conn}}\sim e^{-\mu(T)x}\ , \tag{2.12}$$

where $\mu(T)=O(gT)$.

Ordinary local operators such as the space-space oriented plaquette operator are expected to create AA glueballs, and space-time oriented plaquettes may couple to ϕA glueballs as well.

At very high temperature g becomes small due to asymptotic freedom and we expect two distinct mass scales for excitations in the plasma: $\phi\phi$ and ϕA glueballs with mass gT and multi-A glueballs with mass g^2T. At lower T, g is of order one and we expect these states to mix. However, it seems reasonable that all the masses should scale with T to first approximation, with logarithmic corrections coming from the temperature dependence of g. As we get close to the critical temperature the system becomes more and more nonperturbative and the behavior of masses versus T consequently more and more poorly understood. Since the deconfinement transition is first order, there may be a discontinuous jump in the masses of the color-singlet modes from $T>T_c$ to $T<T_c$. There is no reason to expect any of these modes to become massless.

To complete our discussion of the expected temperature dependence of the screening masses, let us recall that it has been proposed that the phase transition of the plasma be modeled in strong coupling after a classical statistical spin theory with a Hamiltonian:

$$H=-\sum_{(\mathbf{x},\mathbf{y})}L(\mathbf{x})L^\dagger(\mathbf{y})\ ,$$

where $\mathbf{x}$ and $\mathbf{y}$ are nearest-neighbor pairs on a three-dimensional lattice and $L(\mathbf{x})$ is the Wilson line variable.[13] Such a spin theory undergoes a phase transition from an ordered (low-spin temperature) phase to a disordered (high-spin temperature) phase. (The spin temperature is inversely related to the gluon plasma temperature.) The phase transition is first order, but with the introduction of a "magnetic field"

$$H'=-h\sum_{\mathbf{x}}\mathrm{Re}L(\mathbf{x})$$

it becomes second order at a small value $h=h_{\mathrm{cr}}>0$.[14] Thus the phase transition for $h=0$ is expected to reveal some characteristics of critical behavior, in particular, a correlation length that grows sharply near the phase transition. Because the phase transition is in fact first order, the correlation length is bounded from above, however.

III. CALCULATIONAL DETAILS

We now begin a discussion of our numerical simulation. We will first describe our programs, then the operators we

measured, and finally how we analyzed the data.

A. Monte Carlo programs

Two different programs were used during the course of this work. The first program is a modified version of the vectorized code of Barkai, Moriarty, and Rebbi[15] and was run on CDC-205's at Colorado State and Florida State Universities. It uses a ten-hit Metropolis algorithm. The main modification which we made to the original code was to convert the boundary conditions from periodic to skew periodic.[16] This modification results in increased speed because, on a skew-periodic lattice, variables which have identical relative locations in the lattice, regardless of how close they may be to boundaries, are found in identical relative offsets in computer memory. This does not occur when ordinary periodic boundary conditions are used. Thus one can multiply two sets of links throughout the lattice simultaneously without having to reorder one set of links. On a CDC-205, reordering an array involves "gather" commands, which run at one fifth the speed of (32-bit) multiplication. We do not need these commands and so our code is faster: using a ten-hit Metropolis algorithm and 32-bit multiplication on a two-pipe CDC-205, we update one link in around 33 μsec for lattice sizes appropriate to this experiment.

The second program was run on the Boeing Computer Services Cray 1S and XMP computers and on the University of Illinois National Center for Supercomputing Applications Cray-XMP. The program evolved from a scalar SU(3) code by Claude Bernard, altered substantially to optimize vector calculations, and it incorporates a 124-word shift register random-number generator inspired by Douglas Toussaint and the Kennedy-Pendleton version of the Cabibbo-Marinari[17] "quasiheat bath" algorithm for the link update. Three SU(2) subgroups were used in this application of the method. The update speed achieved on the Boeing Cray-XMP was about 38 μsec per link for all the lattice sizes in this analysis. The advantage of the quasiheat bath algorithm over the ten-hit Metropolis algorithm is (as shown by Cabibbo and Marinari[17]) that it results in a reduction in noise, so that approximately half as many sweeps are required to obtain the same statistical accuracy for the measurements we are making.

The final difference between the codes involves the measurement of operators. We are measuring expectation values of operators averaged over time and over two transverse directions as a function of the separation in the third spatial direction from a source. (We will describe these operators more fully in the next section.) Suppose we order the coordinates of the axes from most quickly varying in computer memory to most slowly varying as $xyzt$ with t slowest. The Cyber program measures expectation values as a function of distance in z from a source at fixed z averaged over x, y, and t, while the Cray program measures expectation values at a distance in x from a source at fixed x averaged over the y, z, and t directions. Because we are using skew boundary conditions based on the sequential arrangement of lattice sites in memory, there is a subtle difference between these methods that leads to slight differences in measurements made by the two programs. The differences are finite-size effects and arise from the treatment of variables at the edge of a plane.

TABLE I. Comparison of Cyber and Cray program measurements for Wilson-line expectations as a function of distance d from a source, at $\beta=5.75$, $N_t=4$.

d	Cyber	Cray
1	0.3559(5)	0.3523(6)
2	0.2492(7)	0.2484(8)
3	0.2133(13)	0.2146(13)
4	0.1963(17)	0.1998(15)
5	0.1910(22)	0.1945(19)
	Fitted parameters (3 parameter fits) $d=2-5$	
a	0.1800(39)	0.1861(46)
b	$9.8(9)\times10^{-3}$	$7.7(3)\times10^{-3}$
μ	0.75(7)	0.80(10)
	a parameter from sourceless runs	
	0.176(8)	0.178(3)
	μ parameter (a input from sourceless runs), $d=2-5$	
	0.74(3)	0.66(4)

To see how a difference arises, consider the calculation of an x-y oriented plaquette parallel to a wall at fixed z and at the edge of the lattice. The skew periodicity of the boundary conditions may cause it to include links that are the same as links in the fixed $z\pm1$ hyperplane. This occurs because the site with coordinates $(x,y,z,t)=(x,N_y+1,z,t)$ is identified with the site with coordinates $(x,0,z+1,t)$. On the other hand, the calculation of a y-z oriented plaquette parallel to a wall at fixed x always involves links in the fixed x hyperplane and never in the $x\pm1$ hyperplane. The difference at any rate dies out in the large transverse volume limit. It can be used to test the effects of the choice of boundary conditions on the results.

Both codes were cross-checked against one another and against published measurements of expectation values of various operators.

Tables I and II illustrate the differences in measurements of the two programs. It is apparent that despite the small differences, the fitted masses agree within $1\frac{1}{2}\sigma$.

B. Observables

There are at least two methods for measuring mass gaps in a Monte Carlo simulation: one may measure point-to-point correlation functions of one set of operators with another, or one may introduce a source in one part of the lattice and monitor the asymptotic decay with distance of the disturbance of the source using various operators as antennas.[18] Both these methods have been used with success to measure glueball masses in intermediate coupling in SU(3) lattice gauge theory for $T<T_c$. To date, several groups[19,20] have measured point-to-point correlations out to separations of two or three lattice spacings but no farther. By contrast an extensive source calculation by de Forcrand, Schierholz, Schneider, and

TABLE II. Comparison of Cyber and Cray program measurements for Wilson-line expectations as a function of distance d from a source, at $\beta=6.05$, $N_t=8$.

d	Cyber	Cray
1	0.1530(4)	0.1500(2)
2	0.0839(5)	0.0821(4)
3	0.0634(4)	0.0621(4)
4	0.0539(5)	0.0524(6)
5	0.0484(12)	0.0474(7)
6	0.0450(15)	0.0447(8)
7	0.0437(19)	0.0437(10)
	Fitted parameters (3 parameter fits) $d=3-7$	
a	0.0379(36)	0.0411(18)
b	0.0056(4)	0.0025(10)
μ	0.48(5)	0.63(8)
	a parameter from sourceless runs	
	0.029(3)	0.032(4)
	μ parameter (a input from sourceless runs), $d=3-7$	
	0.35(3)	0.40(+7−4)

Teper[21] has measured correlations over the range of three to ten lattice spacings for $5.5\leq\beta\leq5.9$. We have elected to measure expectation values of operators in the presence of a source which is a constant in time as a function of the displacement of the operator in a spatial direction which is henceforth called z.

One introduces a source into the lattice by modifying the path integral from

$$Z=\int [dU]e^{-S(U)} \tag{3.1}$$

to

$$Z(F)=\int [dU]F(U)e^{-S(U)} . \tag{3.2}$$

An operator expectation value is then

$$\langle\phi(z)\rangle=\frac{\int [dU]F(U)e^{-S(U)}\phi(z)}{Z(F)} . \tag{3.3}$$

We assume that the source is localized to the region $z=0$, and measure the expectation values of operators at a distance z in the z direction from the source, averaged over the x, y, and t directions. We can define a transfer matrix $\mathcal{T}$ with respect to the z axis. Our source modifies the link integration over a hyperplane in z, so it corresponds to a state $|F\rangle$. Then for any Heisenberg state $|G(z)\rangle$

$$\mathcal{T}|G(z)\rangle=|G(z+1)\rangle \tag{3.4}$$

and

$$\langle\phi(z)\rangle=\frac{\langle F(L)|\phi(z)|F(0)\rangle}{\langle F(L)|F(0)\rangle} . \tag{3.5}$$

Now introducing a complete set of eigenstates of $\mathcal{T}$,

$$\mathcal{T}|n\rangle=e^{-\mu_n}|n\rangle , \tag{3.6}$$

putting μ_j in ascending order, and normalizing $\mathcal{T}$ to $\mu_0=0$, we find the numerator and denominator of (3.5):

$$\langle F(L)|\phi(z)|F(0)\rangle=\sum_{n,m}\langle F|n\rangle\langle n|\phi|m\rangle\langle m|F\rangle \times e^{-\mu_n(L-z)}e^{-\mu_m z} , \tag{3.7}$$

$$\langle F(L)|F(0)\rangle=\sum_n |\langle F|n\rangle|^2 e^{-\mu_n L} . \tag{3.8}$$

Approximating the ratio gives

$$\langle\phi(z)\rangle\approx a+b\cosh\mu_1(z-L/2) , \tag{3.9}$$

where the error is exponentially small in the quantities $\mu_1 L$, $(\mu_2-\mu_1)z$, $(\mu_2-\mu_1)(L-z)$, and

$$\begin{aligned} a&=\langle 0|\phi|0\rangle , \\ b&=e^{-\mu_1 L/2}\langle 0|\phi|1\rangle\langle 1|F\rangle/\langle 0|F\rangle . \end{aligned} \tag{3.10}$$

The source method has one great advantage and one great disadvantage compared with the point-to-point correlation method. The great advantage is that it happens that one can measure correlations against the source out to a greater distance than one can measure correlations of two local operators. Perhaps this occurs because fluctuations of $\langle n|F\rangle$ are smaller than those of $\langle 0|\phi|n\rangle$ for small n and so the data from the source method is less noisy than from correlations. We typically begin our fits to the data using (3.9) at a distance $N_z=3$, and extend them to a distance of 6 or 7 lattice spacings from the source.

However, the great disadvantage of the source method is that the coefficients in the expansion (3.7) are not positive definite. The analogous formula for point-to-point correlations is

$$\langle 0|\phi(z)\phi(0)|0\rangle-|\langle 0|\phi|0\rangle|^2=\sum_{n\neq 0}|\langle 0|\phi|n\rangle|^2 e^{-\mu_n z} . \tag{3.11}$$

A positive-definite variational principle applies. Thus fitting the right-hand side to $ae^{-\mu z}$ always results in $\mu\geq\mu_1$ owing to the positivity of the terms. The nonpositivity of the series in the ratio of (3.7) to (3.8) means that no such bound exists, so that if z is not large enough, the mass estimates may have systematic errors of unknown sign. We will describe tests for asymptotic behavior below.

We have chosen as our source the simple structureless wall obtained by setting all x, y, and t links equal to the identity at $z=0$. At $T=0$ such a wall is known to be a source of 0^{++} glueballs. At finite temperature we expect it to be a source of the $T\neq0$ analog of 0^{++} glueballs and of other states as well, such as the "singlet plasmon."

C. Operators

We have measured expectation values of two classes of operators in the presence of a source: nonlocal operators—Polyakov loops (Wilson lines) and local operators (various closed paths of link variables). Among the local operators we have considered are 1×1, 1×2, and 2×2 x-y plaquettes, 1×1 x-t, and y-t plaquettes.

It is already known from $T=0$ work[20] that for $\beta\geq6.0$ 1×1 plaquettes have a uselessly small coupling to one-

glueball states. We can also see the coupling of 2×2 plaquettes weakening at large β. These effects are easily understood as a consequence of the increasing correlation length (and increasing size of a glueball in lattice units) with increasing β. As the continuum limit is approached a physical glueball becomes a very complicated object whose overlap with a simple thin flux loop becomes small.

D. Fitting the data

1. The data set

The data set which we have collected is cataloged in Table III. It consists of many long runs at $N_t=4$ and 6 and shorter runs at $N_t=8$. The simulations consumed about 150 hours of CDC-205 time and 120 hours of Cray time. As in the case of most other glueball calculations, the data are not from a region of β where asymptotic scaling is seen for all observables.

The collection of data was somewhat different in the two programs. The Cyber data are built of a number of runs, each of which consists of a thousand sweeps of the lattice. The first 200 sweeps in each run was discarded, then measurements were carried out every 4 sweeps and averaged. Only the overall average was kept. Errors were determined by making many runs and averaging the measurements from each run. Except for the initial value of β, the starting lattice configuration for the Monte Carlo run was taken from the last configuration of the lattice at a nearby value of β.

The Cray data consists of runs of 5000 and sometimes 10 000 sweeps of the lattice at each value of β with a warm-up run of 200 sweeps discarded. Generally the starting lattice at a given value of β was the final lattice at a neighboring value of β, although in some instances the initial configuration had all links set to one. Measurements were made after each sweep, binned into averages of 50 contiguous measurements, and recorded in a data summary file. An interactive data analysis program running on a VAX carried out further binning and made further cuts as needed. In this way it was possible to determine the autocorrelation length from sweep to sweep and to watch for nonequilibrium trends in the data. Indeed, only near the phase transition did it appear that correlation lengths exceeded 50 sweeps, but even there, they never exceeded 200 sweeps. Thus the practice of discarding the first 200 sweeps was prudent. The finer-grained data sample in the Cray runs also made it possible to explore correlated fluctuations in the expectation values as a function of z. They are discussed below.

2. Likelihood function: Covariance in z

We attempt to fit the data to the functional form (3.9)

$$c(z)=a+b\cosh\mu(z-\tfrac{1}{2}L)\ . \tag{3.12}$$

We can define a best fit as one that minimizes the "naive" χ^2:

$$\chi^2=\sum_i \frac{[c_i-c(z_i)]^2}{{\sigma_i}^2}\ . \tag{3.13a}$$

(c_i and σ_i are the expectation values and errors of an operator c at a distance z_i from the source.) However, a closer examination of our data reveals that there is a strong covariance in the c_i from sweep to sweep. Defining a correlation coefficient for the correlation of the measurement at distance i and distance j,

$$h_{ij}=\frac{1}{\sigma_i\sigma_j}\sum_{k\ \text{sweeps}}[c_i(k)-\langle c_i\rangle][c_j(k)-\langle c_j\rangle]$$

($h_{ij}=1$), we find that h_{ij} can be quite large for $i=j\pm1$—as big as 0.7–0.8 in some cases. (See Table IV.) What is happening is that patches of the lattice are fluctuating coherently over a distance of many lattice spacings.

It was found that the determination of the correlation matrix h_{ij} for correlations of up to 7 values of z was quite stable if the data sample included a couple dozen sets of measurements k. (Clearly if the number of sets of measurements is equal to or less than the number of values of z, h becomes a meaningless singular matrix.)

The pattern of fluctuation or covariance also shown in Table IV is amusing. Diagonalizing h gives eigenvectors characterizing the uncorrelated fluctuation modes. The corresponding eigenvalue gives the degree of fluctuation for that mode. The larger the eigenvalue, the greater the fluctuation. The pattern of eigenvectors looked rather like those of a vibrating string of beads with both ends free. The largest fluctuation was associated with all points shifting in phase. The next largest had one node, the next, two, etc., with the best determined deviation corresponding to the largest number of nodes. There was often a difference as large as a factor of 100 between the largest and smallest variance.

Because the covariance is strong, it is in principle inappropriate to use Eq. (3.13a) as the function to be minimized. Therefore we also fit the data using the "correlated" χ^2:

$$\chi^2=\sum_{ij}h_{ij}^{-1}\frac{[c_i-c(z_j)]}{\sigma_i}\frac{[c_j-c(z_j)]}{\sigma_j}\ . \tag{3.13b}$$

Since we are fitting a smooth curve to the mean data points it is rather unlikely that the best fit gives a pattern of residuals with more than a couple of nodes. Consequently the best-fit value of χ^2 was often anomalously small for the naive count of the number of degrees of freedom. Nevertheless, the 1σ error defined as the region in parameter space over which χ^2 increased by 1 always agreed well with the errors found by partitioning the data and looking at the distribution of best parameter values found in each subset. Therefore, we have confidence in the ability of χ^2, defined in (3.13b), to give a good estimate of the 1σ error in the fitted parameters, but we cannot use χ^2 to give a measure of goodness of fit.

The $N_t=4$ and $N_t=6$ data have been fit using both definitions of χ^2. We found that in all cases the best fit values of μ using the two methods agreed within $1\frac{1}{2}$ standard deviations.

3. Asymptotic behavior

Independent of our choice of definitions of χ^2 (correlated or uncorrelated) we must face the problem of what

TABLE III. Summary of data sample and fitted screening lengths.

									Local operators				
					Sweeps			Wilson	Space-space			Space-time	Mean of
β		Lattice			(thousands)	Program	d	line	1×1	1×2	2×2	1×1	local operator
5.55	4	11	11	13	4.4	QHB	2—6	0.69(1)	0.88(4)	0.90(3)	0.94(3)	0.81(3)	0.89(3)
							3—6	0.78(2)	0.95(12)	1.04(12)	0.96(11)	0.91(10)	0.97(11)
5.60	4	11	11	15	5	QHB	3—7	0.57(2)	0.72(7)	0.75(6)	0.82(7)	0.67(6)	0.74(6)
							4—7	0.59(2)	0.72(18)	0.80(19)	0.90(20)	0.70(13)	0.78(19)
5.65	4	11	11	13	5	QHB	2—6	0.34(1)	0.86(5)	0.87(4)	0.86(4)	0.74(5)	0.83(4)
							3—6	0.27(1)	0.54(16)	0.57(16)	0.66(16)	0.68(14)	0.61(15)
5.70	4	11	11	13	5	QHB	2—6	0.72(4)[a]	1.10(6)	1.12(6)	1.15(6)	1.07(4)	1.11(6)
							3—6	0.72(10)[a]	0.94(28)	1.07(26)	1.19(28)	1.01(21)	1.05(26)
5.72	4	11	11	15	5	QHB	2—7	0.73(2)	1.01(6)	1.07(5)	1.17(5)	1.02(5)	1.07(6)
							3—7	0.63(4)	1.19(28)	1.13(20)	1.20(23)	0.99(14)	1.13(20)
5.75	4	11	11	11	2.4	QHB	2—5	0.66(4)	1.01(12)	1.07(12)	0.99(11)	1.12(16)	1.05(12)
					16	M	2—5	$0.67(^{+12}_{-7})$	1.15(5)		$1.27(^{+7}_{-11})$		1.17(4)
	4	11	11	15	1.8	QHB	2—7	0.68(4)	1.11(11)	1.18(11)	1.17(10)	1.08(8)	1.14(11)
							3—7	0.59(6)					
5.77	4	11	11	15	5	QHB	2—7	0.76(2)	1.14(7)	1.12(6)	1.16(7)	1.13(7)	1.14(6)
							3—7	0.65(6)	1.12(24)	0.92(19)	0.93(21)	0.76(17)	0.93(21)
5.8	4	11	11	11	22	M	2—5	0.78(5)	1.57(.15)		$1.29(^{+9}_{-5})$		1.33(6)
5.9	4	11	11	11	20	M	2—5	0.92(7)	1.31(9)		1.33(6)		1.32(5)
5.95	4	11	11	15	12	M	3—7	$0.50(^{+3}_{-7})$	$1.3(^{+4}_{-2})$		$0.91(^{+15}_{-20})$		1.01(15)
6.0	4	11	11	15	24	M	3—7	0.64(15)	0.6(2)		1.16(40)		0.72(18)
5.70	6	11	11	13	5	QHB	2—6	0.61(1)	0.87(3)	0.88(3)	0.89(3)	0.84(4)	0.87(3)
							3—6	0.63(2)	0.86(10)	0.87(10)	0.94(10)	0.85(11)	0.88(10)
5.75	6	11	11	13	5	QHB	2—6	0.49(1)	0.94(5)	0.96(5)	0.96(5)	0.91(5)	0.94(5)
							3—6	0.47(2)	0.79(15)	0.80(15)	0.74(14)	0.84(14)	0.79(14)
5.75	6	11	11	15	14.2	QHB	2—7		0.93(3)	0.92(2)	0.93(2)	0.93(2)	0.93(2)
							3—7	0.47(1)	0.77(7)	0.78(6)	0.79(6)	0.81(6)	0.79(6)
							4—7	0.46(2)	0.92(22)	1.03(20)	0.93(18)	0.62(18)	0.88(20)
5.80	6	11	11	13	15	QHB	2—6		1.15(4)	1.13(4)	1.11(5)	1.11(3)	1.13(4)
							3—6	0.31(1)	1.15(14)	1.06(12)	0.94(12)	1.08(13)	1.06(12)
5.80	6	11	11	15	15	QHB	3—7	0.31(1)	1.00(9)	0.96(8)	0.96(8)	0.87(2)	0.95(8)
							4—7	0.30(1)	0.94(30)	0.82(25)	0.74(24)	0.73(23)	0.81(24)
5.83	6	11	11	15	10	QHB	3—7	0.25(1)	1.07(17)	1.00(14)	0.87(11)	0.98(12)	0.98(14)
							4—7	0.23(1)					
5.86	6	11	11	15	10	QHB	2—7		1.19(5)	1.18(5)	1.16(4)	1.20(4)	1.18(5)
							3—7	0.31(1)	1.30(16)	1.09(12)	1.00(12)	1.11(15)	1.13(15)
							4—7	0.27(1)					
5.90	6	11	11	15	10	QHB	2—7		1.36(6)	1.35(5)	1.32(5)	1.31(6)	1.34(5)
							3—7	0.48(2)	1.00(22)	1.02(18)	1.04(15)	1.16(20)	1.06(18)
							4—7	0.47(3)					
					18	M	3—7		0.70(9)		1.09(15)		0.80(8)
							4—7	0.41(4)					
5.95	6	11	11	13	5	QHB	2—6		1.43(10)	1.34(8)	1.25(7)	1.35(10)	1.34(8)
							3—6	0.46(3)					
	6	11	11	15	26	M	3—7		1.18(17)		1.21(16)		1.20(11)
6.0	6	11	11	15	28	M	3—7	0.40(6)	$2.20(^{+10}_{-8})$		0.98(20)		1.17(18)
6.05	6	11	11	15	18	M	3—7	0.43(4)					
							4—7		$0.7(^{+3}_{-4})$		0.30(8)		0.32(8)
6.11	6	11	11	15	23	M	3—7	0.42(6)					
6.15	6	11	11	15	8	M	3—7	0.34(2)					
6.2	6	11	11	15	8	M	4—7	$0.41(^{+12}_{-7})$					
5.85	8	11	11	15	5	QHB	2—7		1.13(5)	1.07(4)	0.99(3)	1.16(4)	1.09(4)
							3—7	0.41(2)	0.93(13)	0.90(12)	0.88(13)	0.90(13)	0.88(13)
							4—7	0.42(3)					
5.90	8	11	11	15	10	QHB	2—7		1.22(4)	1.20(4)	1.81(3)	1.16(4)	1.19(4)
							3—7	0.34(1)	1.03(12)	1.04(11)	0.98(11)	0.98(9)	1.01(11)
							4—7	0.33(2)					
5.95	8	11	11	15	10	QHB	2—7		1.31(5)	1.27(5)	1.20(4)	1.20(4)	1.25(4)
							3—7	0.26(1)	1.23(16)	1.11(12)	1.15(11)	1.17(14)	1.17(11)
							4—7	0.24(1)					

TABLE III. (*Continued*).

β	Lattice	Sweeps (thousands)	Program	d	Wilson line	Local operators: Space-space 1×1	Space-space 1×2	Space-space 2×2	Space-time 1×1	Mean of local operator
6.00	8 11 11 15	14.3	QHB	2–7		1.24(4)	1.24(4)	1.20(4)	0.97(13)	1.16(4)
				3–7	0.24(1)	0.98(14)	1.02(12)	1.05(12)	0.97(13)	1.01(13)
				4–7	0.22(1)					
6.05	8 11 11 15	10	QHB	2–7		1.44(7)	1.41(6)	1.32(6)	1.36(6)	1.38(6)
				3–7	0.40(5)	1.20(26)	1.13(20)	1.15(17)	1.24(17)	1.18(20)
				4–7	0.36(6)					
		16	M	3–7	0.35(3)			0.41(7)		
6.075	8 11 11 15	6	M	3–7	0.48(6)					
6.1	8 11 11 15	8	M	3–7	$0.37(^{+9}_{-6})$			0.56(18)		
6.15	8 11 11 15	8	M	3–7	$0.39(^{+5}_{-4})$					
6.17	8 11 11 15	8	M	3–7	$0.31(^{+5}_{-4})$					

[a]Unconstrained fit was used.

constitutes an acceptable fit. Our most serious difficulty is in deciding at what minimum value of z (call it z_0) our data shows an asymptotic exponential. We make this decision by performing fits to the data beginning at $z_{\min}=2$, 3, and 4. We determine z_0 by requiring that the parameters which minimize the fits for $z_{\min}=z_0$ and $z_{\min}=z_0+1$ lie within one or two standard deviations of one another. We typically find that uncorrelated fits which include one nonasymptotic point are dominated by that one low-z point, because that point shows the greatest deviation from the overall constant in the fit and because the error on the lower-z points are typically half as big as the errors on large-z points. Thus one can get a very good fit (in terms of χ^2), which is however misleading as a measurement of an asymptotic mass. A typical fit is shown in Fig. 2.

We found typically that below $\beta=5.9$ and away from the phase transition ($|\beta-\beta_c|\geq 0.5$) asymptotic behavior sets in at $z_0=2$ or 3 for both Wilson lines and local operators. Above $\beta=6.0$ and close to the phase transition we see asymptotic behavior beginning at $z_0=3$ for Wilson lines. For local operators the asymptotic region shifts to $z_0=4$ or (in the case of one-by-one plaquettes) disappears altogether. For example, at $\beta=6.11$, $N_t=6$, our 1×1 plaquette correlation function is flat from $z=3$ to $z=7$.

4. *Error analysis*

We should also note that the parameters in our fits sometimes have a significant nonlinear correlation. Taking errors from the Hessian matrix can be misleading. In all cases we have checked, the correlation is greatest between the parameters b and μ. In Fig. 3 we display a contour of $\chi^2=\chi_{\min}{}^2+1$ in the b-μ plane holding a to its best-fit value for a "typical" fit.

The shape of the contour is easily understood. The values of all our measurements shrink with increasing z. Thus, to preserve a good fit if b is decreased below its

TABLE IV. Typical factor analysis of covariance of the Wilson-line operator as a function of distance from the source wall. The updating algorithm was quasiheat bath in a vectorized, sequential "checkerboard" pattern. In this case $\beta=5.90$, $N_t=6$.

$h_{ij}=$

1.00	0.55	0.42	0.27	0.18	0.10	0.05
	1.00	0.71	0.49	0.29	0.15	0.06
		1.00	0.74	0.52	0.40	0.276
			1.00	0.79	0.62	0.51
				1.00	0.86	0.78
					1.00	0.91
						1.00

	Eigenvalue	$Z=1$	Eigenvectors 2	3	4	5	6	7
1	0.01	0.01	0.04	−0.15	0.18	−0.38	0.76	−0.47
2	0.11	−0.02	−0.06	0.21	−0.54	0.63	0.18	−0.49
3	0.21	−0.06	0.42	−0.73	0.27	0.41	−0.14	−0.19
4	0.32	0.32	−0.66	0.02	0.53	0.19	−0.19	−0.33
5	0.64	−0.79	0.11	0.37	0.36	0.01	−0.18	−0.27
6	1.74	−0.49	−0.54	−0.35	−0.06	0.22	0.35	0.42
7	3.90	0.20	0.28	0.39	0.15	0.46	0.43	0.38

best-fit value, μ must increase, and if b is increased, μ must decrease. For most fits the contours are relatively straight; however, if b can approach zero the allowed values of μ can become very large, leading to a boomerang-shaped contour. We define the uncertainty in μ and b to be the values of μ and b at the extrema of the contour (as shown in the figure).

5. *Constraining the parameter a from independent measurements*

As noted above (3.10), the parameter a is equal to the expectation value of the operator with no source present. Thus, it is tempting to improve the fitting procedure by measuring this expectation value in a separate source-free computation and to constrain the parameter to the measured value. Notice, however, that Eq. (3.9) has unknown source-dependent corrections to the term of order $e^{-\mu_1 L}$, corresponding to a finite-size effect in the length L. These corrections are very likely to be different in the source-free measurement. If μ is as small as $0.3/a$ with $L=15a$, the corrections are $O(1\%)$. Therefore, this procedure is advisable only when either (1) a and its corrections are known rigorously from symmetry arguments or (2) the statistical error in the fitted value of a from the three-parameter fit exceeds $O(1\%)$ substantially. In our application these criteria limited us to constraining a for the Wilson line operator. In that case it is known from $Z(3)$ symmetry arguments that for $\beta<\beta_c$, $a=0$ exactly and for $\beta>\beta_c$, the error in a was typically 5—10% before constraint. For the local operators the errors in a were typically $O(0.1\%)$ or less. With constrained fits the quoted error in the mass parameter μ_1 takes into account the uncertainty in the constrained value of a. Constraining a typically brought about a decrease in the screening mass μ and had the most significant effect near the phase transition. This result is perhaps not surprising, since it is there that it is found that the correlation length is smallest and the greatest distance from the source is required to reveal the asymptotic behavior. Thus at $\beta=5.90$ on the $6\times11\times11\times15$ lattice ($\beta_c=5.85$), an unconstrained fit to Wilson line data from 10000 sweeps at distances 4—7 from the source gave $\mu=0.51\pm0.14$ but a constrained fit gave $\mu=0.32\pm0.02$ in lattice units. At $\beta=5.80$ an unconstrained fit to Wilson line data from 15000 sweeps at distances 4—7 gave $\mu=0.30\pm0.10$, in agreement with the constrained fit, which gives $\mu=0.298\pm0.008$.

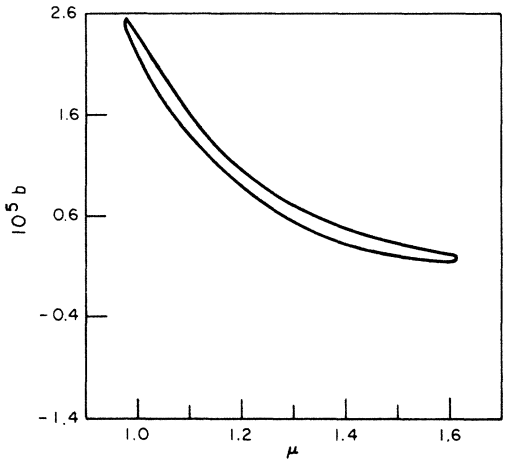

FIG. 3. A typical constant χ^2 contour at the 1σ level for the fitted parameters b and μ at fixed a. Data are 1×1 xy plaquettes from lattice size $11^2\times15\times4$ at $\beta=5.95$.

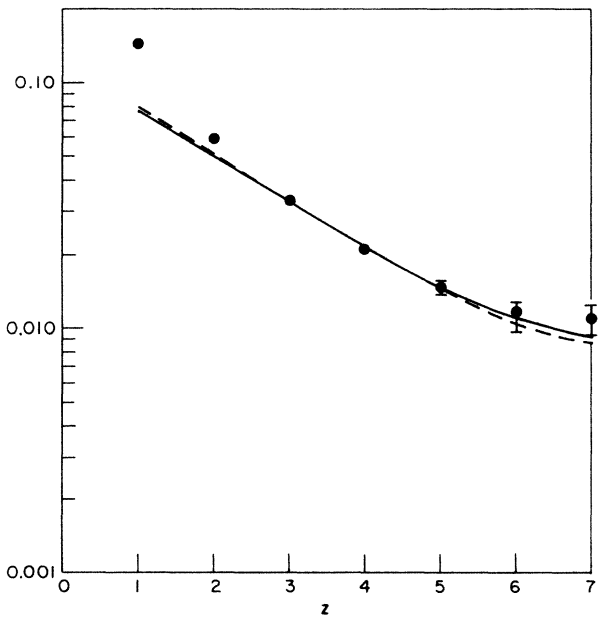

FIG. 2. A typical fit minimizing χ^2 over the range of source distances 3—7. Solid line minimizes χ^2 (3.13a) and dashed line minimizes χ^2 (3.13b). The data are Wilson-line measurements at $\beta=6.05$ on an $11^2\times15\times6$ lattice.

IV. DATA ANALYSIS

There is a rather natural division of our data into correlation functions which are local and ones which are nonlocal (Wilson lines). As the quality of the fits to the two data samples is quite different, we discuss first the Wilson line measurements, and then the local operator measurements.

A. Lattice results

1. *Wilson lines*

We show in Table III our extracted masses μ (in lattice units) for $N_t=4$, 6, and 8 lattices and β ranging from 5.7 to 6.2. For β less than about 6.0 or for $|\beta-\beta_c|\geq0.5$ fits beginning at a distance of two lattice sites from the origin mark the start of the asymptotic regime, and the masses measured starting at $z_0=3$ and 4 are consistent with their values. By $\beta=6.0$—6.1 the asymptotic window has moved to $z_0=3$ but can be checked by $z_0=4$ fits. For the final data point ($N_t=6$, $\beta=6.2$) the fitted mass at $z_0=2$, 3, and 4 are all different and so we have chosen to present the $z_0=4$ value.

We first wish to explore the behavior of μ near the deconfinement phase transition. Since the lattice critical

temperature does not show scaling, it is unjustified to make an extrapolation to the continuum limit. We elect to analyze the results of calculations at different N_t's separately. Graphs of μ vs β for the three N_t values (4,6,8) are shown in Figs. 4–6. The dotted lines show the location of the deconfinement phase transition.

Clearly shown for each N_t is a substantial drop in $\mu_{\rm WL}$ as β approaches β_c from below and a substantial rise just above β_c, followed by a possible slow decrease with increasing β. Whether there is a discontinuity in $\mu_{\rm WL}$ at β_c cannot be conclusively determined from our data, although such an effect is permitted by the first-order character of the phase transition and it is suggested in the data. This behavior is suggestive of a weakly first order, quasicontinuous phase transition in which the correlation length grows substantially, but not without bound.

Our results are not in agreement with those of Fukugita, Kaneko, and Ukawa[19] particularly in that our screening masses do not appear to vanish at the phase transition and the effective string tension does not appear to fall dramatically as β_c is approached from below. However, their calculation had shorter runs (10^3 sweeps) and fit point-to-point correlations at distances as small as one lattice unit.

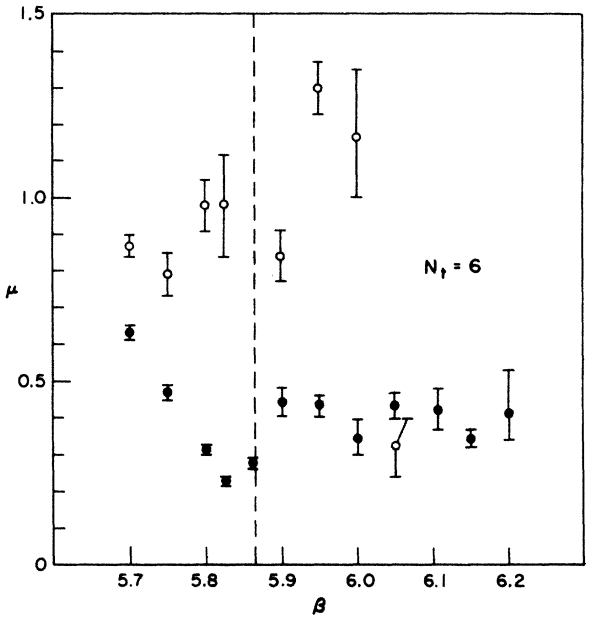

FIG. 5. Same as Fig. 4, but $N_t=6$.

2. *Masses from local operators*

Our results from correlation functions of local operators are much less clear-cut than those from Wilson lines. Consequently we will not even attempt an extrapolation to the continuum and will confine our discussion to masses measured on the lattice.

Generally we find that the masses we extract from correlation functions beginning a distance d from the source show much stronger d dependence than masses extracted from Wilson lines. In many cases it is not possible to obtain stable masses within the constraints of our lattice size. In many cases when we do obtain a d-independent mass, its error bars are about twice as big as the error on a Wilson line mass from the data sample. Also, in many cases, the value of the mass measured from local operators is larger than the mass measured from Wilson lines.

All of these difficulties presumably arise from the fact

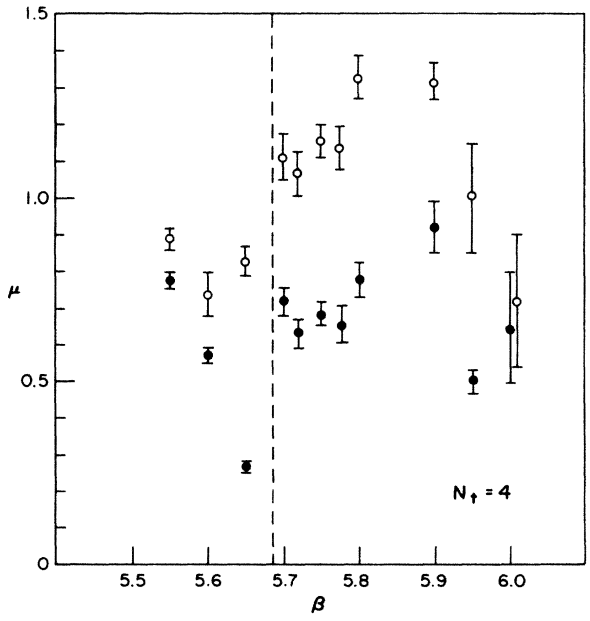

FIG. 4. Graph of lattice mass μ vs β, for $N_t=4$. The dotted line shows the location of the deconfinement phase transition. Closed circles show the masses extracted from Wilson-line measurements, open circles from local operators.

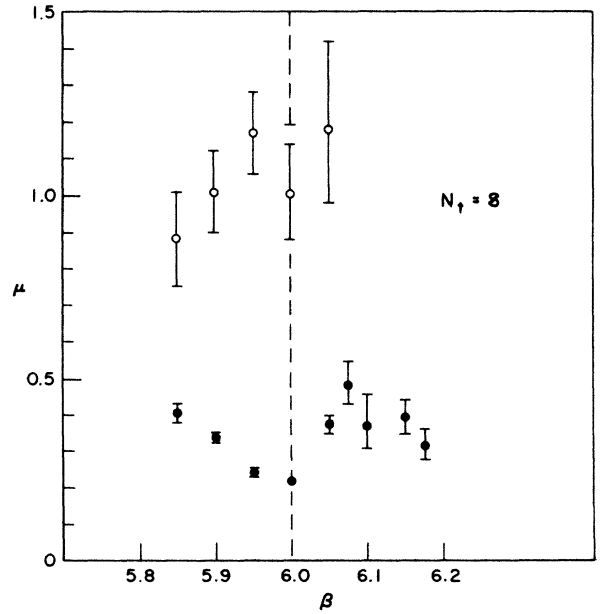

FIG. 6. Same as Fig. 4, but $N_t=8$.

that the local operators we have employed have poor overlap with the lightest excitation of the lattice plasma near $\beta=6$. The magnitude of the b term [see Eq. (3.12)] is always about an order of magnitude below b for the Wilson lines. With our data sample (10000–20000 sweeps per point) a typical error in a correlation function is a few parts in 10^4. This error is about the size of our signal at a separation of 5 or 6 lattice spacings from the source. This fact restricts the window over which we can see a pure exponential: an operator with poor coupling to the lightest excitation in its channel may show its asymptotic behavior only when the signal is lost in the noise.

With these caveats made we present masses μ extracted from fits to the expectation values of operators fit to a single exponential (3.12) where the fit began at a minimum separation from the source. In Table III we show masses extracted from 1×1 plaquettes in the xy plane, 2×2 plaquettes in the xy plane, 1×2 plaquettes in the xy plane, and 1×1 plaquettes in the xt and yt planes. We do not include results of three parameter fits to data at three points $L/2$, $L/2-1$, $L/2-2$: we feel that the data is too noisy there to trust those results. We have not presented any 1×1 plaquette masses for $\beta>6$ since the data is flat (within errors) for $z\geq4$ there.

The reader can see that as a general rule masses extracted from fits to different operators at the same values of β (and beginning at the same minimum distance d) are all roughly equal. Therefore the average mass value of all local operators is given. Since there are strongly correlated fluctuations in the masses among all the local operators, the error in the average value is not less than the errors for the individual operators. The error assigned to the average value has been taken arbitrarily to be the median value of the individual mass errors.

A worrisome point is that the masses that we extract from local operators are consistently higher than the ones we extract from Wilson lines. This is theoretically unsettling for two reasons. First, the analysis of Sec. II suggests that masses from local operators are $O(g^2T)$ in size, smaller than the $O(gT)$ Wilson line masses at sufficiently large T. Second, if the correlation functions were truly asymptotic, they would couple to the lowest-mass excitation of the plasma not forbidden by selection rules. This excitation should presumably be the same one that the Wilson lines couple to, and so one would expect to see the same μ in either case. The only exception would be if the coupling to this lightest mass were anomalously small. To explore further possible evidence for state mixing, we have attempted a three-parameter fit to the two-mass formula:

$$\langle\phi(x)\rangle=a+b_1\cosh\mu_{\rm WL}(z-L/2)+b_2\cosh\mu_2(z-L/2)\ , \tag{4.1}$$

where a is fixed by the separately determined asymptotic value of the local operator, $\mu_{\rm WL}$ is fixed by the mass obtained for the Wilson line, and the parameters b_1, b_2, and μ_2 are varied. Such an expression is expected to be valid if the splitting between the two masses μ_2 and $\mu_{\rm WL}$ is less than the lowest mass. Otherwise there may be a substantial finite L correction to a. As an illustration of this fit, consider the data at $\beta=5.9$ and $N_t=6$. We find, not surprisingly, that the data in the range $z\in[3,7]$ are easily fit with this formula. However, the errors in the mass parameter μ_2 are so large that this procedure should not be trusted to give a useful spectrum. (The mass values were typically in the range $1/a-2/a$ with 50% errors.) Nevertheless, the magnitudes of the fitted parameters b_1 and b_2 are interesting. Recall from (3.10) that the ratio b_1/b_2 is

$$\frac{b_1e^{\mu_{\rm WL}L/2}}{b_2e^{\mu_{\rm WL}L/2}}=\frac{\langle0|\phi|1\rangle\langle1|F\rangle}{\langle0|\phi|2\rangle\langle2|F\rangle}\ . \tag{4.2}$$

Now the state $\phi|0\rangle$ is the state created from the vacuum by the local operator ϕ. The state $|1\rangle$ is the singlet plasmon mode: the state $|2\rangle$ is a higher-mass mode. The ratio of the leftmost terms in the numerator and denominator measures the relative degree to which the state in question overlaps the Wilson-line screening mode. We shall assume the ratio $\langle1|F\rangle/\langle2|F\rangle$ is of order 1 (there is no reason not to expect this to be true of such an extended source). What we find is that for all the local operators the ratio is in the range $\frac{1}{40}$ to $\frac{1}{100}$ for $N_t=6$ and $\beta=5.90$. Thus the data are consistent with a mixing of states at the 1% level. However, if the mass splitting is of order $1/a$ such a contamination would be sufficient to prevent a successful determination of the higher mass with our data for the simple reason that at a distance $z=4a$ a 1% contamination becomes a 50% contamination.

B. Continuum results for Wilson lines

We finally attempt to extrapolate our lattice results for β much greater than β_c to the continuum limit, using the perturbative renormalization group. In the asymptotic limit the bare lattice spacing a is related to the physical temperature through

$$\frac{1}{T}=N_ta \tag{4.3}$$

and to the lattice cutoff Λ_L through the two-loop β function:

$$a\Lambda_L=\left[\frac{8\pi^2}{33}\beta\right]^{51/121}e^{-4\pi^2\beta/33}\equiv f(\beta)\ . \tag{4.4}$$

Thus a lattice of temporal extent N_t and lattice coupling β has a physical temperature

$$\frac{T}{\Lambda_L}=\frac{1}{N_tf(\beta)}\ . \tag{4.5}$$

A mass μ measured in lattice units corresponds to a physical mass

$$\frac{m}{\Lambda_L}=\frac{\mu}{f(\beta)} \tag{4.6}$$

or

$$\frac{m}{T}=N_t\mu \ . \tag{4.7}$$

We face an immediate complication in our analysis in that most of our data comes from β values where neither T_c nor the string tension scale (although $T=0$ glueball masses might). Two groups[22] have recently seen indications of perturbative scaling in T_c/Λ with T_c/Λ_L about 45, on lattices of length $N_t=10$, 12, and 14. The critical coupling at $N_t=10$ is at $\beta_c=6.15$. As all of our data are taken on lattices with $N_t\leq 8$ and only two data points have $\beta>6.15$ we are not likely to be in a scaling region.

A second complication is that we expect that for $T\gg T_c$

$$\frac{m}{T}\propto g^2(T) \tag{4.8}$$

for local operators and

$$\frac{m}{T}\propto g(T) \tag{4.9}$$

for Wilson lines. The variation of the coupling constant with physical temperature obeys

$$\frac{3g^2(T)}{4\pi^2}=\frac{1}{\frac{11}{6}\ln(T/31.3\Lambda_L)+\frac{17}{22}\ln\ln(T/31.3\Lambda_L)} \ . \tag{4.10}$$

Equation (4.10) varies by a factor of $2\frac{1}{2}$ as T/Λ_L runs between 60 and 120. Indeed, if $m=Tg(T)$ then over this range of temperature the mass in physical units remains nearly constant.

These two problems tangle our analysis more than a $T=0$ calculation because we want to address two questions simultaneously: Do our results show continuum behavior? And what is $m(T)$?

In Fig. 7 we plot m/T vs T/Λ for all our data. The three different lattice sizes allow the data to overlap in T/Λ: $N_t=6$ and 8 at $T/\Lambda=60$–65, $N_t=4$ and 6 at $T/\Lambda=80$–85. The data lie in a smooth band which decreases with increasing T/Λ.

Let us try to fit $m(T)=RTg(T)$, using Eq. (4.10), to our data. We restrict ourselves to $T/\Lambda>60$ in hopes of being closer to the asymptotic limit. The fit is shown as the line in Fig. 7. To the eye it looks plausible, but the fit has a χ^2/DF of about 4.6. What is happening, of course, is that the data is not scaling—an unsurprising result.

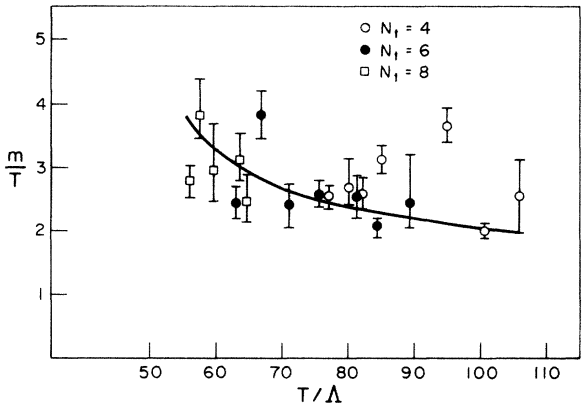

FIG. 7. Graph of m/T vs T/Λ for all Wilson-line data. The curve is a fit to $m(T)=RTg(T)$ using Eq. (4.10).

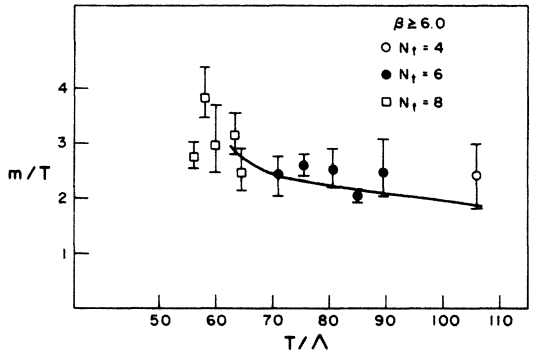

FIG. 8. Same as Fig. 7, except only data for $\beta\geq 6$ are plotted.

We attempt to produce a scaling data set by removing all the points for $\beta<6$. The remaining points are plotted in Fig. 8. The choice $\beta<6$ is arbitrary and represents an attempt to keep only large-β points without throwing out all the data altogether.

We again fit $m(T)/T=Rg(T)$. We find (and show in the figure) $R=0.77\pm0.03$. This time the fit is very good: χ^2/DF$=1.5$ for 10 DF. Finally, we should remark that although Fig. 8 presents strong evidence that the singlet plasmon screening scales like $Tg(T)$, we cannot rule out other behavior. As we have remarked, over the range $60<T/\Lambda<120$ the quantity $Tg(T)$ is nearly a constant,

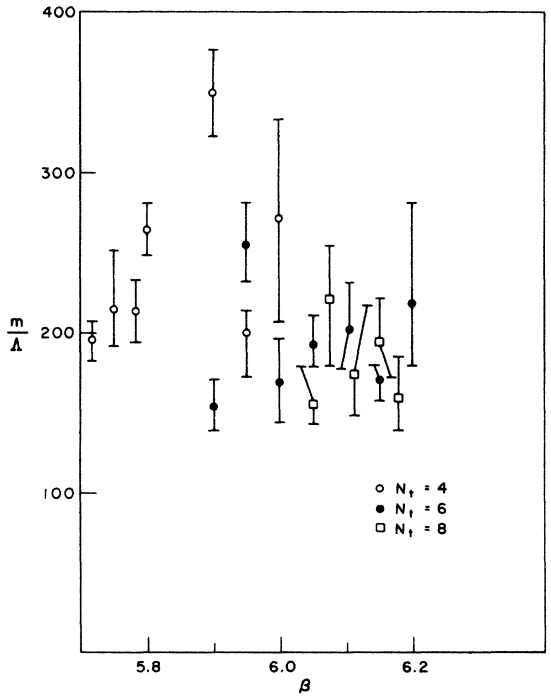

FIG. 9. Graph of m/Λ vs β for all Wilson-line data.

so that even if Eq. (4.6) were true, the quantity m/Λ would be nearly constant in T (or β). We illustrate this point by presenting a graph of m/Λ_L vs β (for all our data) in Fig. 9. Above $\beta=6$, m/Λ_L is roughly a constant, $m \sim 275\Lambda_L$.

V. CONCLUSIONS AND DISCUSSION

We have found in the gluon plasma that there is strong evidence for a sharp increase in the correlation length associated with the Wilson line in the vicinity of the phase transition and that our data is consistent with an approximate scaling behavior $m_{\mathrm{WL}}=(0.77\pm0.03)g(T)T$ at higher temperatures. The Wilson-line screening phenomenon (i.e., singlet plasmon screening) is related to the string tension at zero temperature. Thus it is amusing to piece together a composite sketch of the behavior of the singlet plasmon screening length suggested by our data. The sketch is shown in Fig. 10. It should be stressed that, since our low-β data do not show asymptotic scaling and our measurements do not cover the whole range down to $T=0$, the figure is not to be taken literally.

We have also measured screening lengths for local operators (operators formed from small Wilson loops). Because those operators may excite the singlet plasmon mode for $T>T_c$, but are forbidden by $Z(3)$ selection rules from exciting that mode for $T<T_c$, we are unable to quote a screening mass for this mode for $T>T_c$. At zero temperature this mode is equivalent to the 0^{++} glueball. It is also included in Fig. 10 with the same caveats.

Our study cannot resolve the issue whether the plasma modes are confined or deconfined. Nor does it measure real-time excitations of the plasma. One might be tempted by these results to infer that since the singlet plasmon mode has a large screening length near T_c, that it corresponds to a plasma excitation with a low-gap frequency. However, it is not known whether the singlet plasmon for $T<T_c$ is a propagating mode. It is very likely to propagate for $T>T_c$ since it mixes with the glueball analog mode. Further theoretical work on this interesting question is needed.

Our results have implications for lattice gauge theories on small, asymmetric lattices. Our data span ranges of lattice size and coupling equivalent to those of all but the largest simulations performed to date—and more importantly, to all simulations that measure quantities other than T_c. Our simulation show the presence of lattice excitations in the deconfined phase of SU(3) lattice gauge theory for $\beta=5.7$–6.1 or so with masses of around an inverse lattice spacing. This is not the behavior expected of a free gas of gluons, whether in the continuum or on the lattice. Regardless of whether they persist in the continuum limit of the theory, these excitations will presumably affect (and perhaps dominate) the measurement of all observables over this range of coupling constants and lattice sizes.

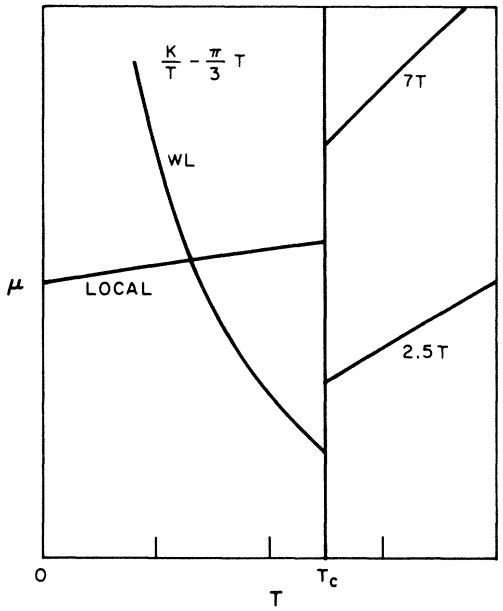

FIG. 10. A schematic summary of our present knowledge of Yang-Mills static screening lengths.

Further work on screening lengths in the gluon plasma should be directed toward increasing lattice sizes in an effort to reach an asymptotically scaling result. Improved methods for reducing noise in the Wilson-line measurements are especially important at larger values of β (Ref. 23). The same analysis should be applied to a study of the quark-gluon plasma. It may also be of interest to study other screening modes with other helicity-parity quantum numbers. We have studied $J^P=0^+$, but by making the source anisotropic, other modes could be sought.

ACKNOWLEDGMENTS

One of us (C.D.) would like to thank John Kogut and the National Center for Supercomputer Applications for a substantial allotment of Cray-XMP computer time during the shakedown phase of the facility. C.D. also thanks Phillipe de Forcrand for helpful discussions of finite-size effects. T.D. would like to thank D. Barkai for providing him with a copy of his program, and the staff of the Supercomputer Computations Research Institute for its support. This work was supported through Grant No. PHY8405648 from the National Science Foundation (C.D.) and by the Department of Energy (T.D.).

[1]For a recent conference proceedings, see *Quark Matter '84*, proceedings of the Fourth International Conference, Helsinki, 1984, edited by K. Kajantie (Lecture Notes in Physics, Vol. 221) (Springer, Berlin, 1985). For a review of QCD calculations, see H. Satz, Annv. Rev. Nucl. Part. Sci. **35**, 245 (1985).

[2]B. Freedman and L. McLerran, Phys. Rev. D **16**, 1130 (1977); **16**, 1147 (1977); **16**, 1169 (1977).

[3]J. Kogut, J. Polonyi, H. Wyld, and D. Sinclair, Phys. Rev. D

31, 3304 (1985).
[4]C. DeTar, Phys. Rev. D **32**, 276 (1985).
[5]For a review, see D. Forster, *Hydrodynamic Fluctuations, Broken Symmetry, and Correlation Functions* (Benjamin/Cummings, Reading, Mass., 1975).
[6]C. Borgs, Nucl. Phys. **B261**, 455 (1985).
[7]T. Appelquist and R. Pisarski, Phys. Rev. D **23**, 2305 (1981); S. Nadkarni, *ibid.* **27**, 917 (1983).
[8]D. Gross, R. Pisarski, and L. Yaffe, Rev. Mod. Phys. **53**, 43 (1981).
[9]J. Polonyi and H. W. Wyld, University of Illinois Report No. ILL-(TH)-85-23, 1985 (unpublished). C.D. thanks Janos Polonyi for discussions of their work.
[10]H. Georgi and S. Glashow, Phys. Rev. Lett. **28**, 1494 (1972).
[11]A. M. Polyakov, Nucl. Phys. **B120**, 429 (1977).
[12]M. Lüscher, K. Symanzik, and P. Weisz, Nucl. Phys. **B173**, 365 (1980); J. Ambjorn, P. Olesen, and C. Peterson, in *Gauge Theory on a Lattice: 1984,* edited by C. Zachos, W. Celmaster, E. Kovacs, and D. Sivers (NTIS, U. S. Department of Commerce, 1984), p. 258.
[13]B. Svetitsky and L. Yaffe, Nucl. Phys. **B210**, 423 (1982).
[14]T. DeGrand and C. DeTar, Nucl. Phys. **B225**, 590 (1983).
[15]D. Barkai, K. Moriarty, and C. Rebbi, Comput. Math. Phys. **32**, 1 (1984).
[16]T. DeGrand and D. Toussaint, Phys. Rev. D **22**, 2748 (1980).
[17]N. Cabibbo and E. Marinari, Phys. Lett. **119B**, 387 (1982); A. Kennedy and B. Pendleton, *ibid.* **156B**, 393 (1985).
[18]G. Parisi, Nucl. Phys. **B180** [F52], 378 (1981); Nucl. Phys. **B205**, 337 (1982).
[19]M. Fukugita, T. Kaneko, and A. Ukawa, Phys. Lett. **154B**, 185 (1985).
[20]See M. Falcioni *et al.*, Phys. Lett. **110B**, 295 (1982); K. Ishikawa, G. Schierholz, and M. Teper, *ibid.* **110B**, 399 (1982); B. Berg, A. Billoire, and C. Rebbi, Ann. Phys. (N.Y.) **142**, 185 (1982); B. Berg and A. Billoire, Phys. Lett. **113B**, 65 (1982); **114B**, 324 (1982); Nucl. Phys. **B221**, 109 (1983); **B226**, 405 (1983); Ph. de Forcrand, G. Schierholz, H. Schneider, and M. Teper, Z. Phys. C **31**, 87 (1986).
[21]Ph. de Forcrand, G. Schierholz, H. Schneider, and M. Teper, Phys. Lett. **152B**, 107 (1985).
[22]S. Gottlieb, J. Kuti, D. Toussaint, S. Meyer, B. Pendleton, and R. Sugar, Phys. Rev. Lett. **55**, 1958 (1985); Norman H. Christ and Anthony F. Terrano, *ibid.* **56**, 111 (1986).
[23]Ph. de Forcrand and C. Roiesnel, Phys. Lett. **151B**, 77 (1985).